Fluid-Composite Structure-Interaction in Underwater Shock Simulations

B. Özarmut[1], A. Rühl[1], B. Hennings[1], O. Nommensen[1], A. Paul[1]

[1]thyssenkrupp Marine Systems GmbH, Werftstraße 112-114, 24143 Kiel, Germany

1 Introduction

Fiber reinforced plastics (FRP) and sandwich components are widely made use of in today's submarines owing to their advantages such as high strength-to-weight ratio and durability in marine environment over conventional submarine building materials. Fig. 1 shows a state-of-the-art conventional submarine with an upper deck consisting of mostly composite components.

Nevertheless, the characteristic material properties of the FRP and sandwich components increase the complexity of numerical modeling and require a thorough investigation of suitable fluid-structure-interaction methods, for example, in the case of an underwater explosion (UNDEX). LS-DYNA offers various coupling mechanisms enabling to observe the effects of such a phenomenon on structures. Some of these modeling approaches can be listed as follows:

- Coincident meshing of Lagrangian elements used for modeling both structure and water
- Interaction of Eulerian (water) and Lagrangian (structure) elements by means of a penalty-based coupling algorithm
- Application of Underwater Shock Analysis (USA) code integrated in LS-DYNA

Each of the mentioned modeling approaches has advantages and limitations in different usage scenarios, and the engineer should be aware of them to choose the most suitable one for the problem dealt with.

Fig.1: A state-of-the-art conventional submarine with an upper deck consisting of mostly composite components

The present paper provides an overview on the UNDEX phenomenon as well as its Finite Element modeling and focuses on the suitability of the mentioned fluid-structure-interaction methods available in LS-DYNA considering the response of the FRP structures.

2 Underwater Explosion (UNDEX)

The effects of underwater explosions on submerged structures are of great importance for the design of modern submarines. A comprehensive understanding of many aspects is required for analyzing this phenomenon. The sequence of events following an underwater explosion is given in [1] as follows:

- Detonation
- Shock wave propagation
- Bubble pulsation

Detonation of an explosive, such as (trinitrotoluol) TNT and pentaerythritol tetranitrate (PETN), can be described as an exothermic chemical reaction converting the explosive material into very high temperature and pressure gas. A highly compressed gas bubble and a steep fronted shock wave are formed as a result of the sudden energy release. The detonation wave travels rapidly through the explosive material and upon arrival of it at the water boundary, the high pressure gas compresses the surrounding water. Since water is compressible, the resulting pressure in the water is then transmitted radially outward as a compressive shock wave propagating with a velocity that is several times the speed of sound in uncompressed water. The velocity of the shock wave falls down to the acoustic level after reaching a distance of about 2-3 times the radius of the charge [2]. Fig. 2 illustrates an underwater explosion and the formation of the resulting steep shock front. As mentioned in [3], the pressure-density relationship becomes nonlinear for very high-pressure amplitudes leading to higher gradients of the pressure-density curve. Due to these higher gradients, the shock wave propagation velocity increases in the corresponding areas, which then induces a very steep shock front.

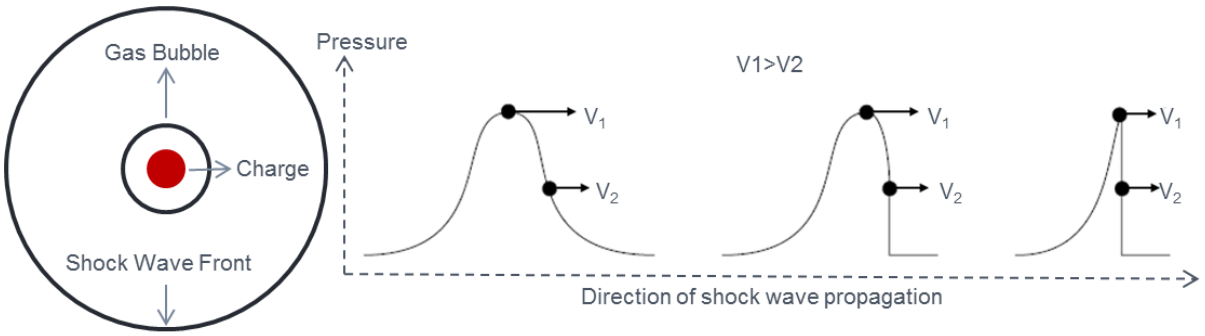

Fig.2: Underwater explosion (left) and formation of the steep shock front (right)

In free water, the shock wave pressure decays exponentially. At a certain distance from the detonation point, the following empirical formulation can be used to approximate the exponential decay behavior of the shock wave profile

$$p(t) = p_{\max} e^{-\frac{t}{\theta}} \tag{1}$$

where $p_{\max}$ and θ represent the peak pressure and the decay constant, respectively, that depend on the explosive. The pressure profile resulting from a spherical shock wave is proportional to the charge weight and inverse of the distance from the charge. The rate of decay is described by the so-called decay constant, which is equal to the time required for the peak pressure to fall down to a value of $p_{\max}/e$. These parameters can be defined for TNT by the following equations as explained in [4]

$$p_{max} = 52{,}4 \cdot \left(\frac{\sqrt[3]{W}}{R}\right)^{1{,}13} \text{ in MPa} \tag{2}$$

and

$$\theta = 0{,}084\sqrt[3]{W} \cdot \left(\frac{\sqrt[3]{W}}{R}\right)^{-0{,}23} \text{ in ms} \tag{3}$$

where W and R are the charge weight and the distance from the charge, respectively.

The exponential decay of the shock wave pressure approximated by Eq. (1) holds true for a time period of at least one decay constant. However, it starts to deviate from the real shock wave pressure profile since a slower rate of decay is observed afterwards [1,5]. The discrepancy after a time period of one decay constant is shown in Fig. 3 by means of the computed and approximated shock wave pressure profiles obtained for TNT.

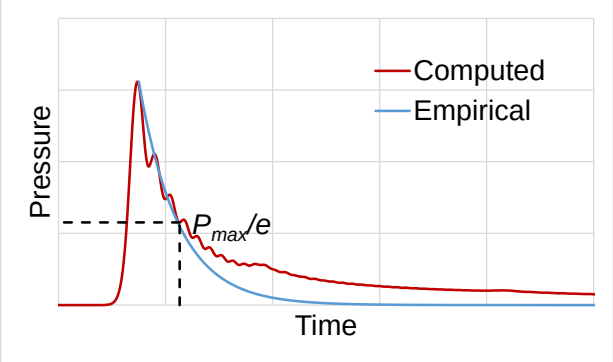

Fig.3: Comparison of the computed and approximated shock wave pressure profiles for TNT

While the shock wave propagates in water, the highly compressed gas bubble expands because of the pressure difference to the surrounding water. The expansion continues beyond the equilibrium hydrostatic pressure due to the inertia of the outward flowing water. Upon reaching its maximum radius, it begins to contract until the gases inside the bubble cannot be compressed anymore and the contraction is rapidly reversed causing a secondary wave around 10-15% of the initial shock wave. This motion of the gas bubble is usually named as bubble pulsation and, as the name suggests, it is oscillatory. Since the bubble pulsation is at least two orders of magnitude slower than the initial shock wave [6], a numerical analysis investigating both phenomena requires a great deal of computational cost. The surface effects of the mentioned steps of an UNDEX are shown in Fig. 4 together with the corresponding animations. The first photo on the left is the spray dome caused by the closure of the bulk cavitation. The shock wave reflected from the water surface is a tensile wave causing bulk cavitation just below the water surface. When the bulk cavitation zone closes, the so-called spray dome is formed. As the second photo shows, the spray dome takes a more conical shape while the gas bubble expands. The water column reaches its maximum when the gas bubble is at its minimum (third photo). The radial breakout of the first plume at an early and a later state is shown in the last two photos. The dark color during the radial breakout of the plume is due to the explosive products being released above the water surface.

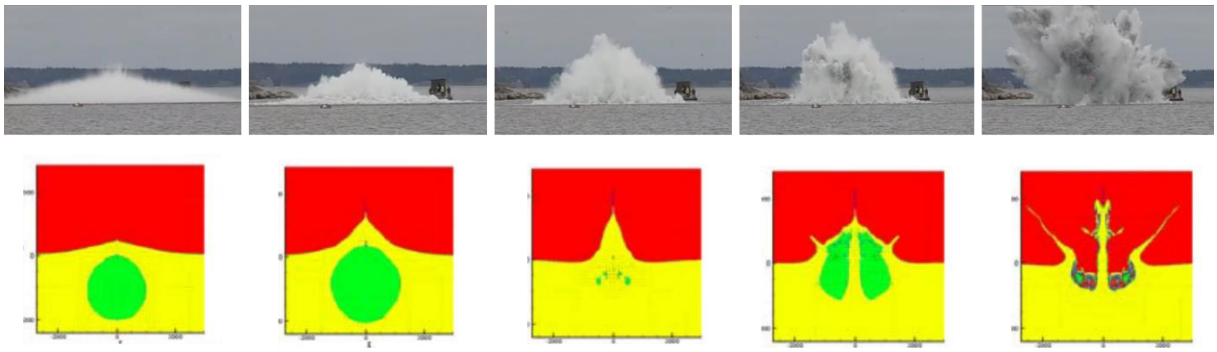

Fig.4: The above-surface effects caused by an UNDEX (animations from [2])

The present work focuses on the effects of initial shock wave on an FRP sandwich panel by investigating the modeling of the fluid-structure-interaction (FSI) and does not account for the influence of gas bubble pulsation.

3 Use Case

The use case is an UNDEX event where a composite panel is positioned in water 5 m away from the charge (PETN). The composite sandwich panel in the current investigation has a square form with 1 m edge length. It consists of a thick hard foam core and two thin laminate skin layers comprised of glass fiber reinforced plastics (GFRP). This type of panel construction provides high bending stiffness with overall low density and thereby produces buoyancy. The panel is mounted in an aluminum frame with the help of a rubber block for a reliable positioning in the water. Multiple pressure gauges are used to investigate the shock wave propagation both at the shock-faced and shadow side of the panel, and they are positioned at a depth aligned with the center of the panel. Table 1 shows the positions of the pressure gauges evaluated for the present panel. PG1X stands for the pressure gauges positioned at the shock-faced side while PG2X indicates the pressure gauges positioned at the shadow side of the panel.

Table 1: Positions of pressure gauges

Pressure Gauges				
Gauge	PG11	PG12	PG21	PG22
Distance [cm]	30	15	15	30

4 Numerical Modeling

The numerical modeling involves the generation of an appropriate discretization, choosing suitable material models and element types, and defining the fluid-structure-interaction (FSI) that can reflect the deformation behavior of the panel as correctly as possible while keeping a good balance between accuracy and computational cost. The following subsections explain concisely the numerical modeling of the panel as well as the FSI modeling approaches.

4.1 FE Model of the Structural Components

The FE model of the structural components includes different discretizations and element formulations. Fig. 5 shows the composite sandwich panel and its FE model along with the aluminum frame and the rubber block. The thin FRP top layers of the panel were modelled by means of thick shell elements. The respective element formulation allows multiple layers to be represented in an element via through-thickness integration points, which significantly reduces the computational cost while capturing the bending response correctly. Furthermore, the assumed strain reduced integration rule handles both shear locking and hourglass problems. One thick shell element in thickness direction was used to model each of the top layers. Therefore, the shear distribution was assumed to be parabolic by setting TSHEAR=0 in the **`*PART_COMPOSITE_TSHELL`** keyword. The constant stress solid element formulation has been used to model the hard foam core, the aluminum frame and the rubber block. Three elements were used to represent the total thickness of the foam core while two elements in thickness direction were modelled for the rubber block. As no significant deformation was expected for the aluminum frame, it was modelled with only one element in thickness direction. The meshes of the components mentioned above are coincident.

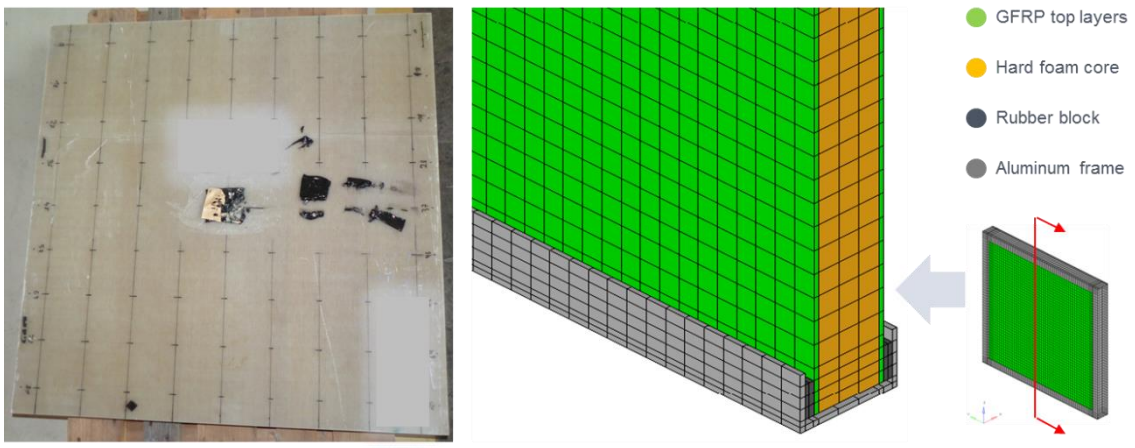

Fig.5: The composite sandwich panel and the rests of the fixation strips (left) and a cross section view of its FE model along with the aluminum frame and the rubber block (right).

The material models used for the components mentioned above, except for the hard foam core, were either ***MAT_ELASTIC** or ***MAT_ORTHOTROPIC_ELASTIC** depending on the characteristics of the used materials. The hard foam core was modeled by means of a user-defined material model (UMAT) as a strain-rate dependent crushable foam.

It should be noted that the same FE model has been used in all simulations in order to keep the number of factors as low as possible, so that the influence of FSI modeling can be better recognized.

4.2 Fluid Modeling and Approaches for Fluid-Structure-Interaction

The water surrounding the panel was modelled with the material model ***MAT_NULL** along with the equation of state ***EOS_GRUENEISEN**. The Gruneisen equation of state defines pressure for compressed materials as

$$p = \frac{\rho_0 C^2 \mu\left[1+\left(1-\frac{\gamma_0}{2}\right)\mu-\frac{a}{2}\mu^2\right]}{\left[1-(S_1-1)\mu-S_2\frac{\mu^2}{\mu+1}-S_3\frac{\mu^3}{(\mu+1)^2}\right]^2} + (\gamma_0 + a\mu)E \tag{5}$$

where C is taken as speed of sound in the corresponding medium and S_1, S_2, and S_3 are unitless coefficients. a stands for the first order volume correction to the so-called Gruneisen gamma γ_0. These parameters were defined in the respective simulations as shown in Table 2.

Table 2: Parameters of ****EOS_GRUENEISEN*** *for sea water*

C	1435 m/s
S_1	2.56
S_2	-1.9086
S_3	0.227
γ_0	0.5

The amount of water required to be modeled depends on the UNDEX scenario to be simulated and the chosen FSI modeling approach. Fig. 6 gives an overview on the models compared in this numerical investigation. The outer boundaries of the water were kept constant in the coincident Lagrange and the ALE approaches. The simulation with the USA code does not require the water to be modeled.

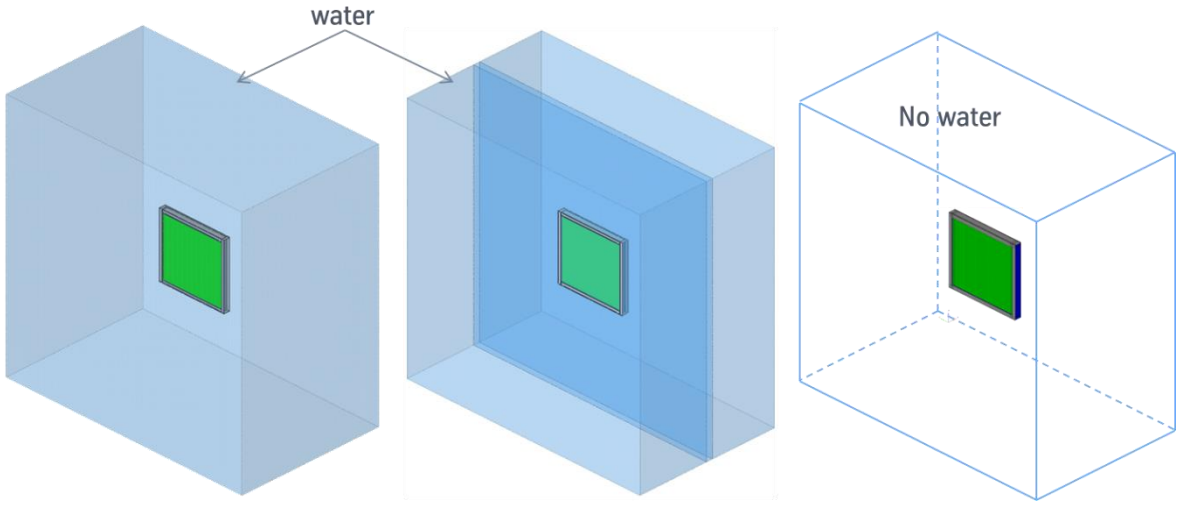

Fig.6: FE models of the simulations with the ALE method (left), the coincident Lagrange (middle) and the USA code (right)

It must be kept in mind that the material model ***MAT_ELASTIC_FLUID** is a similar one but should not be used for problems including shock as it assumes that the speed of sound is constant and the viscosity term works as a kind of numerical damping dependent on many parameters and material constants.

4.2.1 Coincident Meshing via Lagrangian Elements

In this modeling approach, the FE model of the structural parts and the water were coincident. The water discretization was generated by gradually increasing the element size in all directions away from the panel, which led to an element size of water varying between 5 mm and 50 mm. The advantage of this approach is that the FSI occurs naturally through coincident meshes and it can adequately describe the flow of water under certain loading conditions, which becomes, otherwise, a disadvantage. Although the composite sandwich panel has a simple geometry making it easy to generate the water mesh, it can be significantly more difficult and complex depending on the outer contour of the structure. Furthermore, the shock wave propagation might be disturbed if the water mesh is not uniform in the direction of the shock wave. The constant stress solid element formulation ELFORM 1 has been used in the modeling of water. The FE model including the water mesh is shown in Fig. 7. In the section view, it is clearly seen how the nodes on the outer surface of the structural parts are meshed coincident to the water mesh.

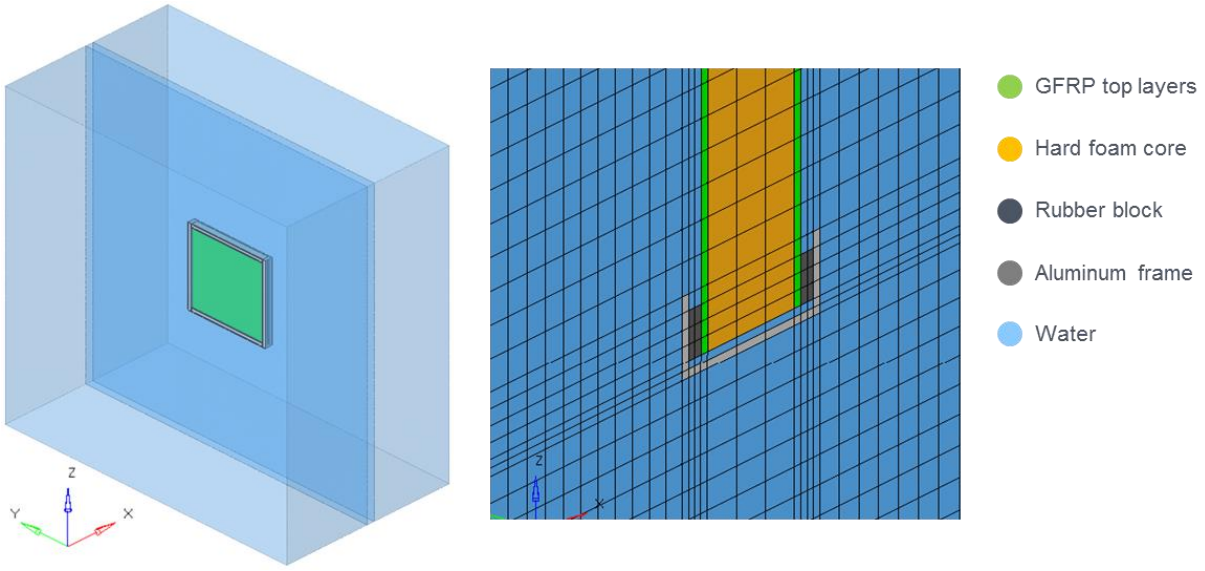

Fig.7: FE model including the Lagrangian water (left) and a cross section view of it (right)

The pressure histories were obtained through the keyword ***DATABASE_HISTORY_SOLID** by selecting the elements corresponding to the positions of the pressure gauges given in Table 1. The surfaces of the water model perpendicular to the direction of the shock wave have been fixed considering the symmetry conditions. This kind of a boundary condition reflects the slip condition (no flow through normal direction). Single point constraints are applied to the node sets by means of the keyword ***BOUNDARY_SPC_SET**. The surface at the shadow side of the panel in the direction of the shock wave was defined as a non-reflecting boundary by means of the keyword ***BOUNDARY_NON_REFLECTING.** This is done to prevent artificial wave reflections from contaminating the results.

4.2.2 Arbitrary-Lagrange-Euler (ALE)

In this modeling approach, there is no necessity to have water elements as small as the ones created for the panel and the other parts as they can overlap other elements. This is for the current calculation the most important advantage. In general, the ALE formulation shows its usefulness in cases where a large deformation is expected. This is due to the fact that an ALE mesh can move arbitrarily in space while material flows through it. An Eulerian mesh, on the other hand, is fixed in space while letting material flow through it. The water mesh has been defined as Eulerian in the current calculation. A uniform Eulerian mesh was created with an element size of 30 mm, which is coarser near the panel and finer at the water boundaries compared to the FE model created with the previous approach.

Even though there is only one ALE material (water) in the current model, the multi-material element formulation ELFORM 11 has been used along with vacuum for the volume allocated by the panel and the connected parts, into which material may be transported. In this way, it is prevented that two

materials do not simultaneously allocate spatially the same volume. A segment set that defines the outer surfaces of the elements representing the structural parts was filled with vacuum via the keyword ***INITIAL_VOLUME_FRACTION_GEOMETRY**. Vacuum was realized by assigning a material density significantly smaller than that of air in the material model ***MAT_VACUUM**.

The FE model including the water mesh is shown in Fig. 8. In the section view, it is clearly seen that the nodes on the outer surface of the structural parts are not connected to the water mesh.

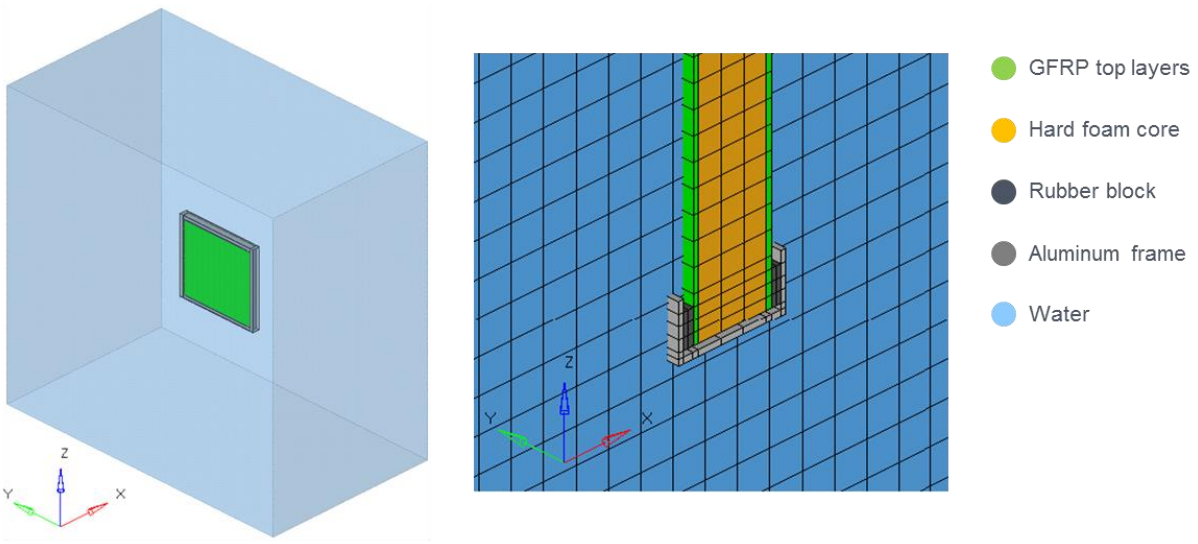

Fig.8: FE model including the Eulerian water (left) and a cross section view of it (right)

The FSI between the Eulerian mesh of the water and the Lagrangian mesh of the structural parts was established by the keyword ***CONSTRAINED_LAGRANGE_IN_SOLID.** The underlying coupling algorithm is a penalty based one that tracks the relative displacement between fluid and structure. The pressure histories were obtained through the keyword ***DATABASE_TRACER** by entering the respective coordinates.

On the contrary to the previous approach, the slip condition on the outer surfaces of the water mesh, except the ones in the direction of the shock wave, was realized by using the keyword ***ALE_ESSENTIAL_BOUNDARY.** The surface at the shadow side of the panel in the direction of the shock wave was defined as a non-reflecting boundary by means of the keyword ***BOUNDARY_NON_REFLECTING.** This is done to prevent artificial wave reflections from contaminating the results.

4.2.3 Underwater Shock Analysis (USA) Code

The Underwater Shock Analysis (USA) routine is a boundary element method code for problems involving underwater fluid-structure-interaction. It is based on doubly asymptotic approximations (DAAs), which are time dependent differential equations for the characterization of transient acoustic fluid-structure-interaction. Since the DAAs represent the water surrounding a structure in terms of wet-surface response variables, there is no need for generating an FE model for the surrounding water. For the current work, the computational saving achieved by leaving out the FE model of the water is the most important advantage of the USA code coupled with LS-DYNA.

The USA code requires a separate input deck, in which the user must provide problem specific conditions, such as the definition of the incident pressure, the charge location, the standoff point, the closest point on the structural wet surface to the charge, the fluid properties and code relevant settings. Various methods are available for defining the incident pressure. The curve option has been employed for a more reliable comparison with the other FSI modeling approaches mentioned above. With this option, the spatial decay of the pressure amplitude is described by 1/R spherical spreading. Another important setting is the form of the DAA fluid-structure interaction equation. It has been observed that the results depend strongly on the selected DAA formulation.

The coupling with LS-DYNA is defined by the keyword ***BOUNDARY_USA_SURFACE**, a segment set containing the whole wetted surface. All segment normals have to be directed to the water. All gaps in the FE model of the structural parts shown in Fig. 5 were filled with Lagrangian water elements in order to avoid numerical instabilities. The modified FE model is shown in Fig. 9.

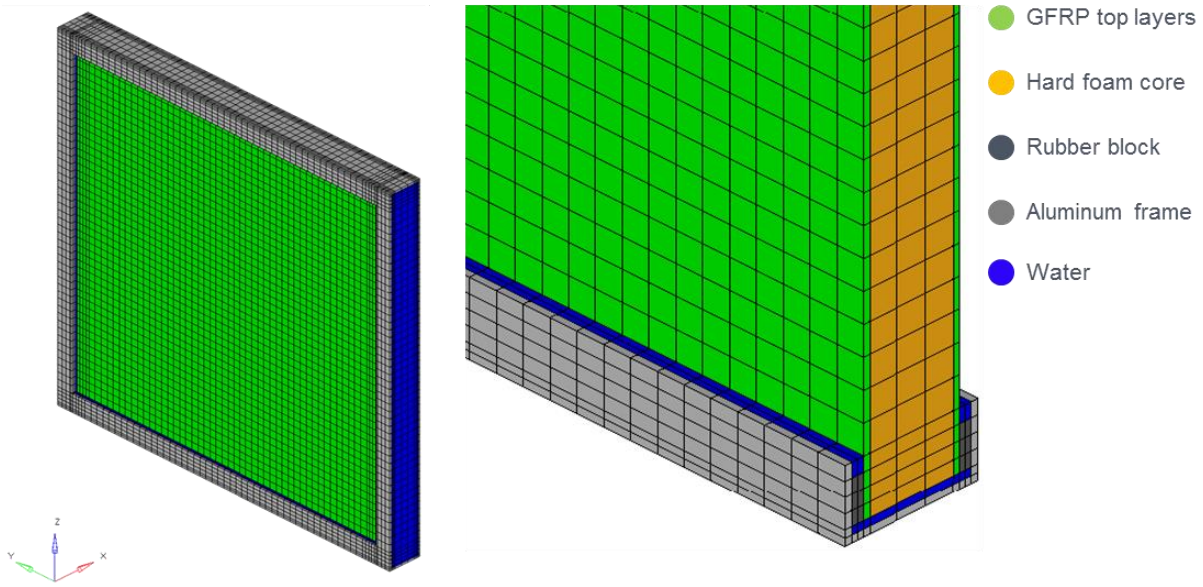

Fig.9: FE model used in the simulations with the USA code (left) and a cross section view of it (right)

4.3 Loading - Shock Wave

Detonation of a spherical charge induces a spherical shock wave that has different characteristics compared to a planar shock wave. If a wave is emitted by a planar source, the energy released by the source is conserved. Thus, it is expected that the pressure amplitude remains the same until hitting an object. On the other hand, as mentioned in section 2, the pressure amplitude resulting from a spherical shock wave is proportional to the charge weight and inverse of the distance from the charge.

With an increasing ratio between the standoff distance and the size of the object in the direction perpendicular to the charge, a spherical shock wave might be assumed as a planar one. In the current configuration, the uppermost and the bottommost points of the panel are hit by the shock wave only 0.0175 ms later than the center of the panel assuming that the speed of sound is at the acoustic level throughout the whole standoff distance. In this case, it is reasonable to use a planar wave as long as the energy attenuation can be correctly represented.

As explained earlier in section 2, the approximation function given in Eq. (1) has a limited range of validity. Furthermore, Eq. (2) and (3) are defined for TNT. Thus, instead of working with the TNT equivalent of PETN, the propagation of the shock wave was simulated by means of a 2D axisymmetric model comprised of Arbitrary-Lagrange-Euler (ALE) elements. In this modeling technique, the explosive is ignited with the keyword ***INITIAL_DETONATION**, in which the detonation point is defined. The detonation and burning of the explosive (PETN) are then modeled by the material model ***MAT_HIGH_EXPLOSIVE_BURN**. In this material model, it is required to define the mass density, the detonation velocity and the Chapman-Jouget pressure of the explosive material. These are defined for PETN as shown in Table 3.

Table 3: Material data of PETN explosive [7]

Density	1770 kg/m^3
Detonation velocity	8300 m/s
Chapman-Jouget pressure	33.5 GPa

The material model ***MAT_HIGH_EXPLOSIVE_BURN** requires an equation of state in order to describe the evolution of the explosive after ignition. The Jones-Wilkins-Lee (JWL) equation of state, implemented as ***EOS_JWL** in LS-DYNA and used in the current investigation, defines the pressure as

$$p = A\left(1 - \frac{\omega}{R_1 V}\right)e^{-R_1 V} + B\left(1 - \frac{\omega}{R_2 V}\right)e^{-R_2 V} + \frac{\omega E}{V} \tag{4}$$

where V and E are the relative volume and the internal energy density per initial volume. A, B, R_1, R_2 and ω are material constants that are defined for PETN in Table 4.

Table 4: Material constants for PETN [7] as input in ***EOS_JWL**

A	617 GPa
B	16.926 GPa
R_1	4.4
R_2	1.2
ω	0.25
E_0	10.1 GPa

The contour plots of the pressure distribution at different simulation times are shown in Fig. 10. The fringe scale of the plots was set to the same minimum and maximum values to make the attenuation of the shock wave visible.

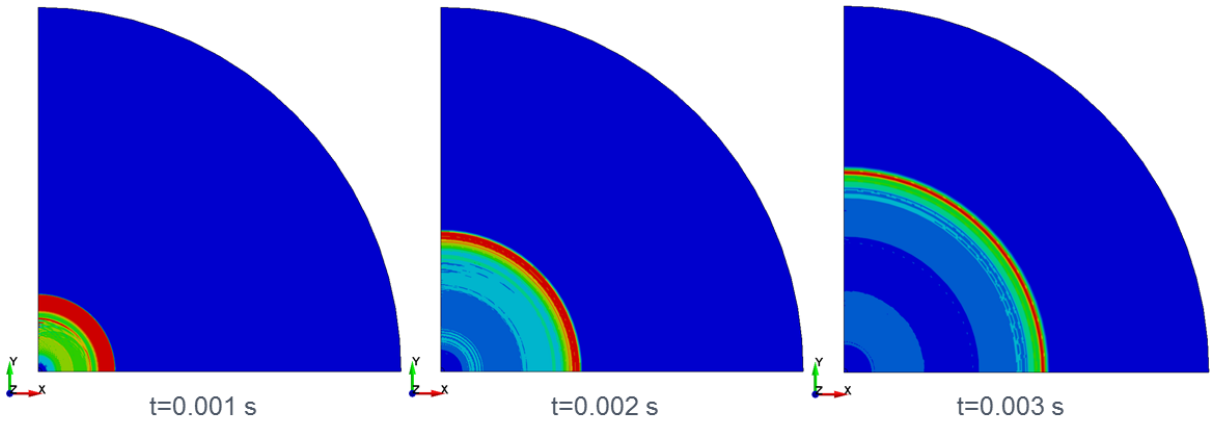

Fig.10: Shock wave propagation in 2D-ALE simulation

The pressure profile obtained from the 2D ALE simulation at the distance where the FE model of water in the 3D simulation starts was applied as a distributed pressure load to the segment sets defined in the relevant 3D simulations (see section 4.2.1 and 4.2.2). LS-DYNA also offers mapping from 2D-ALE to 3D-ALE. This is a more accurate and efficient way of simulating an underwater explosion as the spherical spreading of the shock wave is better described. However, for the sake of a more reliable comparison between the modeling approaches for which an FE model for water was generated, application of a planar wave has been preferred. The further attenuation of the shock wave in the 3D model was assumed to be partially realized through the numerical dissipation caused by the discretization of the water.

In the simulation with the USA code, the pressure profile was applied right at the surface of the panel in order to eliminate the spatial spreading effect of a spherical shock wave. As a result, the pressure amplitude remains comparable to the other two modeling approaches, which only have numerical dissipation.

5 Results

In section 5.1, the pressure-time histories computed with the coincident Lagrange and ALE modeling approaches are validated with experimental results. As the USA code cannot deliver any histories for water, all considered approaches are compared with each other in section 5.2 by means of the pressure-time histories of an element representing the hard foam. All simulations were performed with LS-DYNA R10.1 on four cores. Table 5 shows the simulation times.

Table 5: Simulation times for different FSI modeling approaches

FSI Modeling Approach	Simulation Time [s]
Coincident Lagrange	5869
ALE	19281
USA	475

5.1 Comparison of Pressure Histories in Water

As shown in Fig. 11 and Fig. 12, the first peak of the shock wave and the cavitation are well captured with both modeling approaches. The subtle difference is caused by the planar wave assumption. The shock wave descends with increasing distance from the charge in the test, but there is only little reduction in the pressure amplitude in the simulations because of the numerical dissipation. The slight reflection from the panel before cavitation is not visible in the simulations. The reason might be the coarse discretization. As the speed of sound in the GFRP top layers is higher than that of the water and given that the GFRP top layers are very thin, a significantly finer discretization is required to depict the reflection from the GFRP top layers. After the period of cavitation, the pressure histories have a considerably high discrepancy. This is again due to the selected boundary conditions and the planar wave assumption, which do not allow any attenuation in the reflected waves except the numerical dissipation. However, the trend is well captured and this is important for performing a reliable comparison of the FSI approaches through the foam, explained in section 5.2. Fig. 13 and Fig. 14 show the pressure-time histories at the shadow side of the panel. The pressure begins to descend earlier in the test than the simulations. Nevertheless, the trend is well captured, indicating that the shock wave propagation through the panel is correctly realized. The abnormal oscillation seen in Fig. 14 is a measuring issue.

Both FSI modeling approaches deliver similar results. The deviation between the pressure-time curves could be due to the difference in the discretizations.

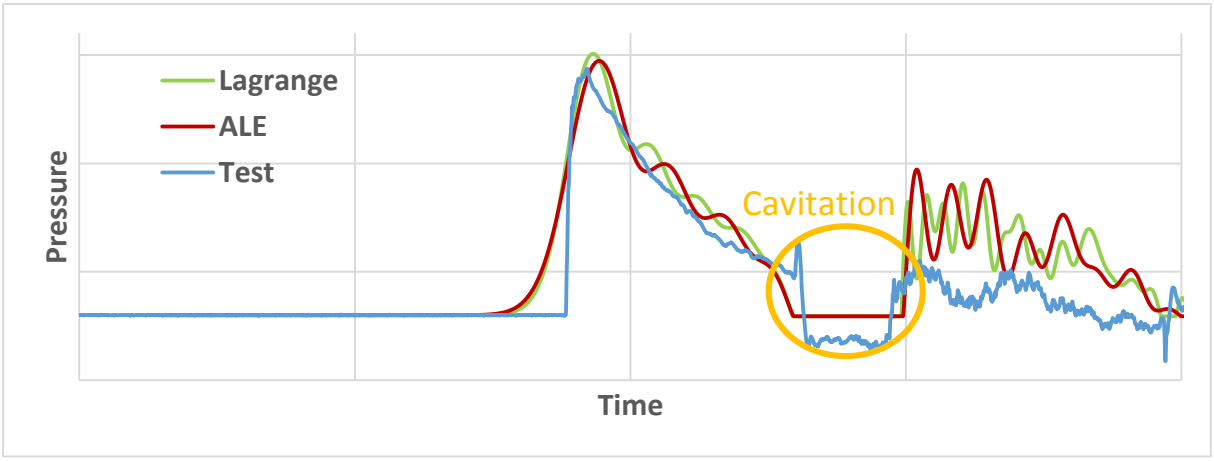

Fig.11: Pressure-time histories obtained at PG11 (300 mm at the shock-faced side of the panel)

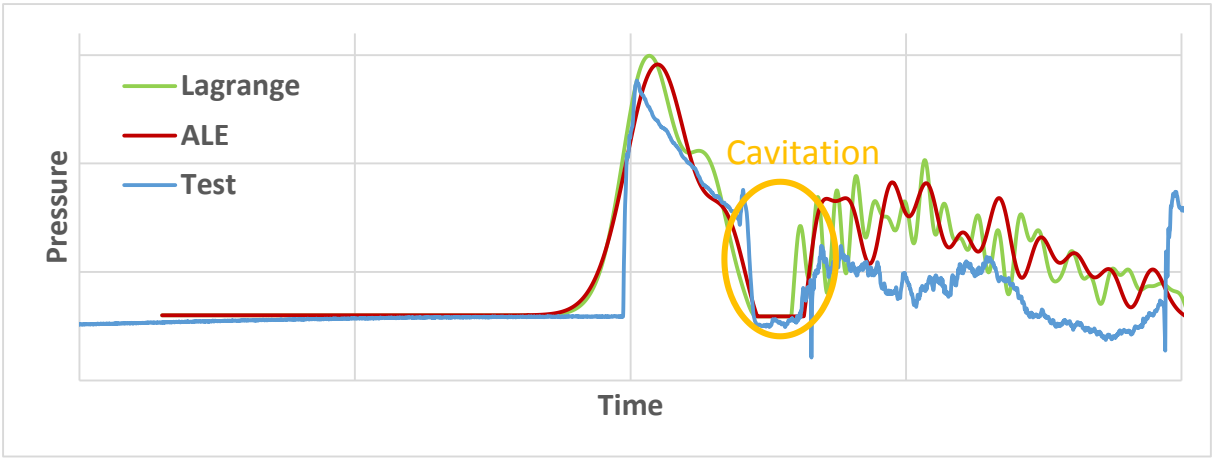

Fig.12: Pressure-time histories obtained at PG12 (150 mm at the shock-faced side of the panel)

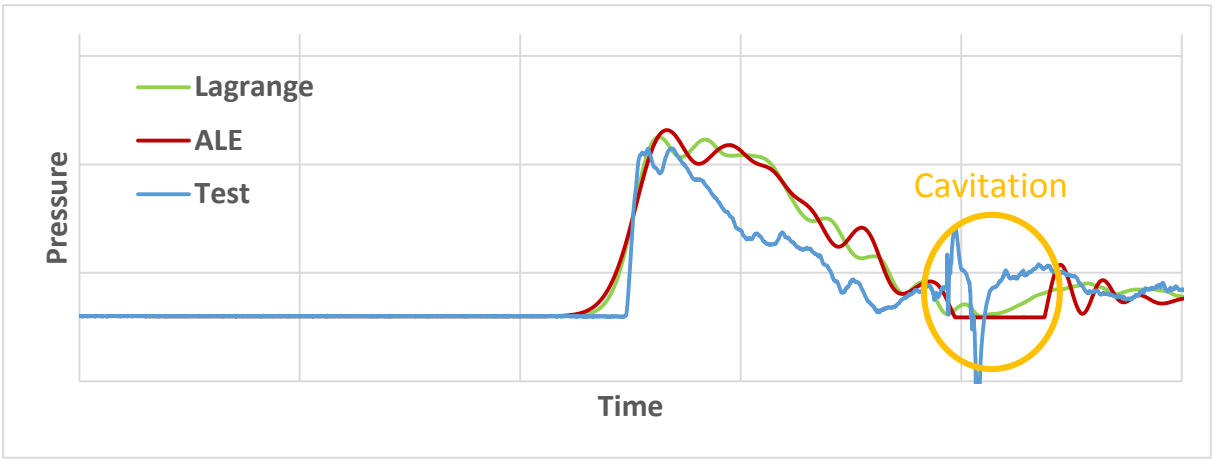

Fig.13: Pressure-time histories obtained at PG21 (150 mm at the shadow side of the panel)

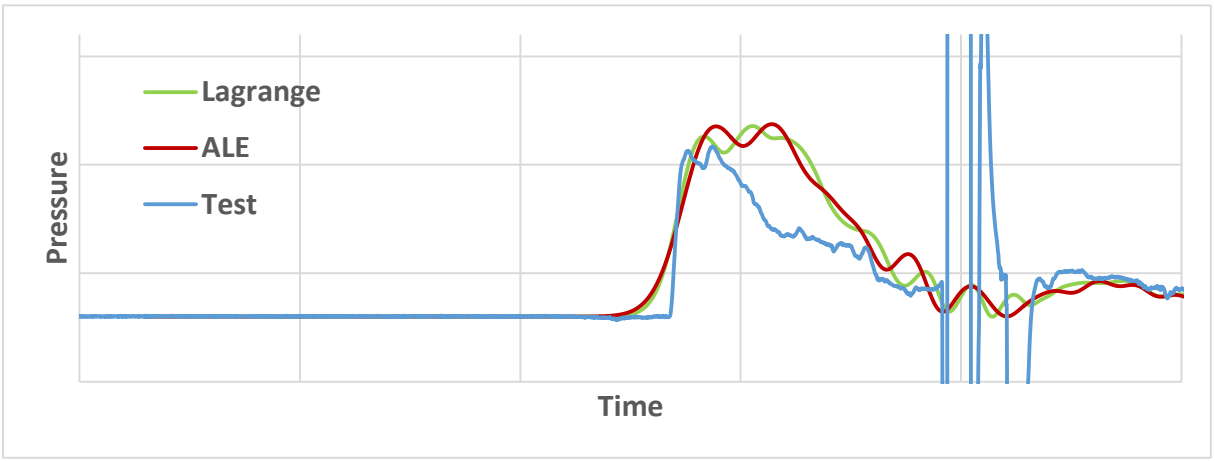

Fig.14: Pressure-time histories obtained at PG22 (300 mm at the shadow side of the panel)

5.2 Comparison of Structural Response

The structural response of the panel was compared by considering a hard foam element at the center of the panel (both through thickness and in plane). Fig. 15 shows the pressure-time histories obtained by means of all mentioned approaches. Although there is no way to say which one of the modeling approaches describes the propagation of the shock wave better through the panel, the pressure-time histories computed with the coincident Lagrange and ALE approaches are very similar. The simulation performed with the USA code shows the same trend in the pressure-time history. A second peak is visible in all simulations. This is due to the reflection of the shock wave from the GFRP layers and the occurrence time of it appears to be related to the FSI at the shadow side of the panel.

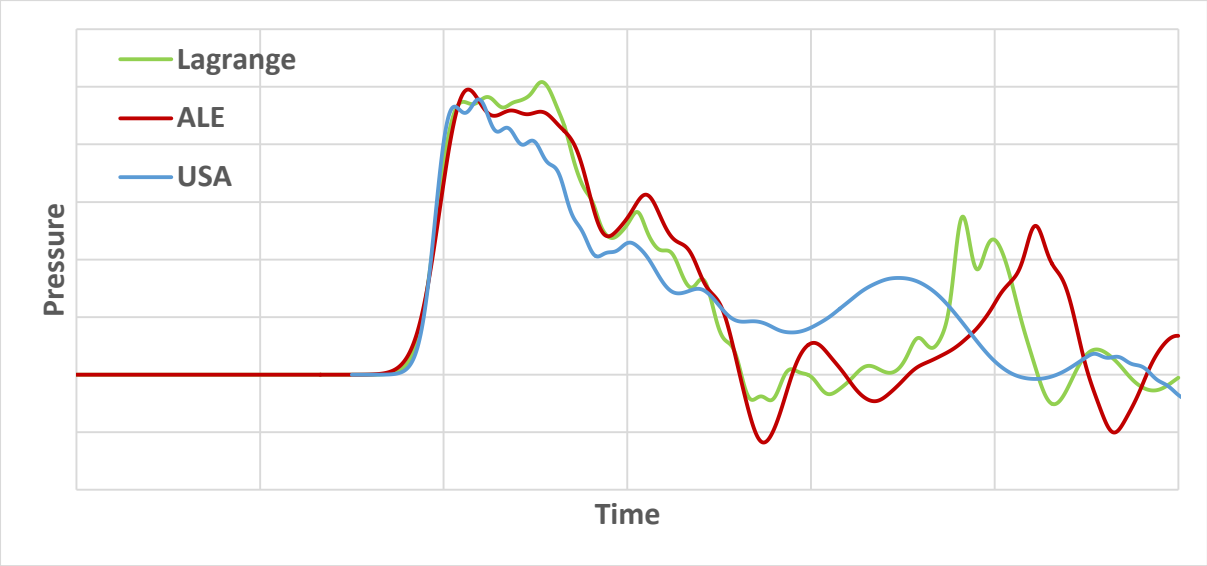

Fig.15: Pressure-time histories obtained at an element representing the hard foam at the center of the panel (both through thickness and in plane)

6 Summary

An overview on the UNDEX phenomenon together with its modeling considering the FSI was presented in the current investigation. Beginning with the detonation of the charge, the realization of the loading condition and its effects on a composite sandwich panel were explained. Different FSI modeling approaches, such as coincident meshing of Lagrangian elements, coupling Eulerian water elements to Lagrangian structure elements, and use of the USA code linked with LS-DYNA, were compared to each other through pressure-time curves of some elements both in the water and the panel. The resulting pressure-time curves showed that there is a slight difference between the Lagrangian and Eulerian methods, but the computational cost is significantly higher in the case of the ALE method. Nevertheless, it should kept in mind that a comparison in terms of simulation times depends strongly on the problem and the applied settings.

By means of the pressure histories of an element representing the hard foam core, the suitability of the USA code for the shock wave propagation through composite sandwiches was tested. Based on the comparison with the other approaches, it has been observed that the USA code can become an alternative for cases where significant amount of water has to be modelled. The computation time is reduced by at least one order of magnitude if the water is not modeled. As the underwater shock behavior is subject to current research projects, further investigation regarding the submarine structures can be found in [8,9].

7 Literature

[1] Cole, R. H.: "Underwater Explosions", Princeton University Press, 1948
[2] Costanzo, F. A.: "Underwater Explosion Phenomena and Shock Physics", Proceedings of the IMAC-XXVIII, 2010
[3] Riedel, W., et al.: “Engineering and Numerical Tools for Explosion Protection of Reinforced Concrete”, International Journal of Protective Structures, 2010
[4] Swisdak, M. M.: “Explosion Effects and properties: Part II – Explosion effects in water”, tech. report, Naval Surface Weapons Center, 1978
[5] Mäkinen, K.: "Underwater Shock Loaded Sandwich Structures", PhD Thesis, Royal Institute of Technology, Sweeden
[6] Best, J. P.: “The Dynamics of Underwater Explosions”, PhD Thesis, University of Wollongong, 1991
[7] Dobratz, B.M., Crawford, P.C.: “LLNL Explosives Handbook”, University of California, 1985
[8] Rühl, A., et al.: “Bolted Joint Connections of FRP-Components in Submarines Subjected to Underwater Shock”, 12th European LS-DYNA Conference, Koblenz, Germany, 2019
[9] Rothaug, T.: HDW Class 206A Shock Trials - Numerical Simulations, UDT Europe Conference Proceedings, 2013